The following publication Yuechuan Lin, Wei Jin, Fan Yang, Yanzhen Tan, and Hoi Lut Ho, "Performance optimization of hollow-core fiber photothermal gas sensors," Opt. Lett. 42, 4712-4715 (2017) is available at https://doi.org/10.1364/OL.42.004712.

Performance optimization of hollow-core fibre photothermal gas sensors

YUECHUAN LIN,[1,2] WEI JIN,[1,2,*] FAN YANG[1,2], YANZHEN TAN[1,2], HOI LUT HO[1,2]

[1]*Photonic Sensors Research Laboratory, Department of Electrical Engineering, The Hong Kong Polytechnic University, Hong Kong, China.*
[2]*Photonic Sensors Research Laboratory, The Hong Kong Polytechnic University, Shenzhen Research Institute, Shenzhen, China.*
**Corresponding author: eewjin@polyu.edu.hk*

Received XX Month XXXX; revised XX Month, XXXX; accepted XX Month XXXX; posted XX Month XXXX (Doc. ID XXXXX); published XX Month XXXX

We report performance optimization of hollow-core photonic bandgap fibre (HC-PBF) photothermal gas sensors. For HC-1550-02 fibre, the photothermal phase modulation coefficient is found independent of the pump modulation frequency for up to ~330 kHz, and it starts to drop quickly to ~10% of the maximum value for frequency ~a few MHz. With a 1.1-m-long HC-PBF in a modified fibre Sagnac interferometer by the use of a 3x3 loop coupler, the lower detection limit of ~67 ppb C_2H_2 is achieved, which go down to ~18 ppb with 145s integration time. The stability of the system was tested over ~5 hours and signal fluctuation was < 1%. The optimized interferometry system could remain comparable sensitivity while operates in a stabilized plug-in-play concept, which is more suitable for practical applications. © 2017 Optical Society of America

OCIS codes: *(060.0060) Fiber optics and optical communications; (060.2310) Fiber optics; (060.4005) Microstructured fibers; (060.5295) Photonic crystal fibers; (060.2370) Fiber optics sensors; (300.6430) Spectroscopy, photothermal.*

xxxxxxxxxx

All-fibre gas sensors based on laser absorption spectroscopy (LAS) have attracted considerable attention over the past 15 years. In addition to the unique selectivity and high sensitivity of LAS, the use of optical fibres as sensing elements (gas cells) as well as light transmission cables would enable sensors with smaller footprint, remote detection capability, immunity to electromagnetic interference (EMI) and possibility of distributed sensing along a single optical fibre. D-shaped optical fibres were studied as evanescent wave gas cells but the fraction of evanescent field in air is too small to conduct practically useful experiments [1]. Microstructured or holey optical fibres, including photonic crystal fibres and suspended-core fibres, have a much larger fraction of evanescent field in the air-holes (a few to over 10% of the total modal power)[2, 3], and have been experimentally demonstrated for gas detecting with good sensitivity [4, 5]. The development of hollow-core photonic bandgap fibres (HC-PBFs) makes it possible to guide a light mode in an air-core with attenuation as low as a few dB/km [6, 7]. The fraction of modal power in the air-core can be as large as 95%, enabling strong light-gas interaction in the hollow-core over a long distance [4, 5]. HC-PBFs can be coiled down to a couple of centimeters without obvious increase in loss and hence are ideal for making compact all-fibre gas cells. Detection of various gases such as methane, acetylene and ammonia have been experimentally demonstrated with HC-PBFs from centimeters to over ten meters but the detection is limited to ppm level, due mainly to the multi-path (modes and polarizations) interference noise that could be significantly larger than the absorption signal [2, 8-11].

Recently, we demonstrated a highly sensitive gas detection technique with HC-PBFs [12]. Instead of measuring the transmission loss, the technique detects the absorption-induced phase change due to photothermal (PT) effect. A pump and probe configuration is used: absorption of a modulated pump beam induces localized heating that modulates the phase of a probe beam propagating through the same gas sample, and the phase modulation can be detected with high precision by the use of optical interferometry [13]. The use of a HC-PBF enables the phase modulation efficiency by over 4 orders of magnitude over the free-space approach [12, 14, 15].

In this Letter, we report the results of our further experimental and theoretical investigations on the frequency-dependent characteristics of PT phase modulation in a HC-PBF and demonstrate stable operation of a HC-PBF gas sensor over a period of several hours, an important step toward the practical application of the PT HC-PBF sensors.

The frequency-dependent characteristics of PT phase modulation is experimentally studied with the setup shown in Fig. 1. It is similar to the one used in [12] but the modulation format of the pump is different. Instead of wavelength modulation, here the wavelength of the pump is fixed to the center of the P(9) absorption line of C_2H_2 while its intensity is modulated by an acousto-optic modulator (AOM) periodically. Such an arrangement ensures the PT phase modulation is at the pump modulation frequency and makes it easier to determine the frequency response of the phase modulation by simply analyzing the spectrum of the interferometer output with an electrical spectrum analyzer (ESA).

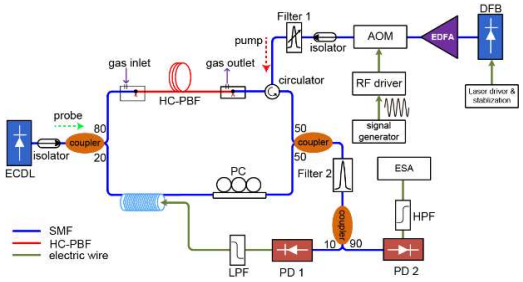

Figure 1, Experimental set-up for the measurement of frequency-dependent PT effect in HC-PBF. LPF: low pass filter; PD, photo-detector; HPF: high pass filter; Filter 2: optical filter used to filter out the residual pump beam; Filter 1: optical filter used to filter out the ASE noise accompanying the EDFA.

The gas cell used is a 0.62-m-long HC-PBF with its two ends fusion-spliced to single-mode fibres (SMFs), and it is placed in the sensing arm of the Mach-Zehnder interferometer (MZI). 15 side holes were made along the HC-PBF gas cell by the use of a femtosecond laser-drilling technique [16] and 7500 ppm C_2H_2 gas buffered by N_2 filled the HC-PBF gas cell by self-diffusion via the side holes. The interferometer is stabilized at quadrature by active servo-control [12] which enables efficient and linear conversion from PT phase modulation into the interferometer output intensity. By varying the frequency of pump intensity modulation and recording its corresponding magnitude of the output signal, the frequency response can be obtained. Fig. 2 shows the measured phase modulation (the red circles) against the pump modulation frequency. The vertical axis is normalized against the maximum value that occurs approximately at ~30 kHz. The magnitude of PT phase modulation shows no significant change at low frequency, drops to ~90% of the maximum value at ~330 kHz, and reduces quickly from ~440 kHz to ~ 2 MHz. This frequency-dependent characteristic is very different from that in a free-space system in that the PT phase modulation frequency is approximately linearly dependent on frequency even down to a few kHz level [13].

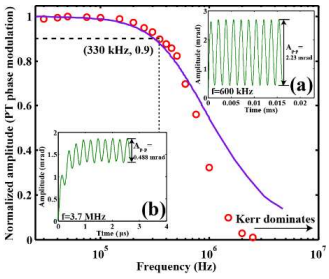

Figure 2 frequency dependent of PT effect in HC-PBF. The violet solid line is the results of numerical simulation while the red dot is the measured results. The inset (a) and (b) are the simulated results in time domain for modulation frequency of 600 kHz and 3.7 MHz, respectively.

Theoretical investigation of the phase modulation was also carried out by modeling the HC-PBF with a cylindrical tube with its inner diameter equals to the diameter of the hollow-core. Under the assumption that the heat conduction of gases within hollow-core is the dominant heat transfer process, the dynamics of PT phase modulation may be studied by use of the following heat conduction equation [15]:

$$\rho C_p \frac{\partial T}{\partial t} + \rho C_p \mathbf{u}\cdot\nabla T = \nabla\cdot(\kappa\nabla \mathrm{T}) + Q \qquad (0.1)$$

where $\rho(=1.165\,kg/m^3)$ is the density, $C_p(=1040\,J/(\mathrm{kg}\cdot\mathrm{K}))$ the specific heat capacity and $\kappa(=0.0256\,W/(\mathrm{m}\cdot\mathrm{K}))$ the thermal conductivity of buffer gas (N_2). $\mathbf{u}$ is the velocity field. For a sinusoidally modulated pump beam, the heat source Q may be expressed as:

$$Q(\mathrm{r},\mathrm{t}) = \alpha C \mathrm{I}_{pump} \exp(-2\mathrm{r}^2/\mathrm{w}_{pump}^2) \times[1+\cos(\omega_p \mathrm{t})]/2 \qquad (0.2)$$

where I_{pump} is the peak pump intensity and w_{pump} is the beam radius of pump beam. α is the absorption coefficient of target gas sample at 100% relatively concentration and C is the gas concentration in volume ratio. ω_p is the modulation frequency of pump beam.

The computed phase modulation as function of time for pump modulation frequency of 600 kHz and 3.7 MHz are respectively shown in insets (a) and (b) of Fig. 2. The parameters are identical to the experimental condition with peak pump power of ~14.6 mW except that the gas concentration is 100 ppm. The peak-to-peak magnitude of PT phase modulation (A_{p-p}) at 600 kHz is about 4 times larger than that at 3.7 MHz. For higher modulation frequency, the heat conduction could not catch up with the heat generation, resulting in an obvious rise of DC level at the onset of pump modulation as well as smaller value of A_{p-p} at the steady state. The computed phase modulation magnitude (normalized against its maximum value) as function of frequency is also shown in Fig. 2. The modulation efficiency drops to 90% at ~330 kHz, agreeing well with the experimental results. At higher frequencies, the deviation between the computed and the experimental results become significant due to probably the Kerr effect occurring in the section of SMF within the MZI via which the high pump power is delivered to the HC-PBF gas cell. In the experiment, the length of SMF in the sensing arm is about 10 m, and the pump power in the SMF is estimated to be ~45.6 mW in the input and ~9.1 mW in the output. The Kerr phase modulation is estimated to be ~1.2 mrad, which is opposite in sign to the PT phase modulation and results in smaller total modulation as observed in the experiments. The magnitude of PT phase modulation at 2.5 MHz is estimated to be ~4 mrad with 14.6 mW peak pump power and 7500 ppm C_2H_2 gas concentration. At less efficient PT effect, the PT phase modulation tends to cancel out the Kerr-induced phase modulation at one specific modulation frequency.

As discussed in [15], this frequency at turning point may be determined by the core radius of HC-PBF and thermal conductivity of buffer gas N_2 . The results of frequency-dependent PT effect would be a basic criteria of modulation frequency choice in our further system design.

The MZI configuration requires active servo-control to maintain stable operation at quadrature and adjustment and calibration is needed every time when the system is switched on and when the HC-PBF gas cell is replaced. This is not preferred for practical applications and the use of electronic feedback also compromises its ability for remote detection and for operating in higher EMI environment.

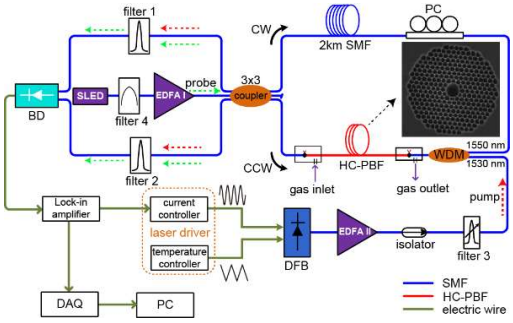

Figure 3, the experimental set-up of PT gas spectroscopy. Filter 1&2: two DWDM (fixed at 1553.33 nm) to filter out the residual pump beam; Filter 3: tunable filter to filter the undesired ASE noise; BD: balanced detector; DAQ: data acquisition card; PC: personal computer.

To overcome this limitation, we studied the use of a Sagnac interferometer for phase detection. A Sagnac interferometer is a single fibre interferometer in which two counter-propagating beams travel in the same fibre but different direction. To maximize the sensitivity, a constant phase bias of $\pi/2$ may be introduced with a 3x3 loop coupler in combination with a balanced detector (BD) [17], as shown in Fig. 3. The three output ports of the 3x3 coupler have a fixed 120° phase difference and the use of balanced detection makes the output probe signal directly proportional to the PT phase modulation in the HC-PBF gas cell. In our experiments, an amplified, wavelength-modulated DFB laser was used as the pump source, which generates PT phase modulation in the HC-PBF. The probe beam is divided into clock-wise (CW) and counter-clock-wise (CCW) direction. We use a 2-km SMF as the delay fibre so that the CW and CCW beams pass through the HC-PBF with a time delay of $\sim 10\ \mu s$ and the phase difference is maximized by operating at the proper frequency of Sagnac loop, i.e. ~ 50 kHz for first harmonic detection, which is also within the optimum frequency (<330 kHz) for PT phase modulation as discussed above.

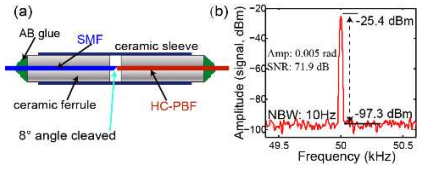

Figure 4, (a) schematic drawing of gas cell; (b) ESA output of PZT phase modulator (amplitude of 0.005 rad).

The probe light is from a broadband super-luminescent diode (SLED, bandwidth of ~41 nm, central wavelength at 1545 nm) filtered by a low finesses Fabry-Perot (FP) filter (center wavelength of 1553.33 nm, bandwidth ~1.2 nm, corresponding to a coherent length of ~ 636 μm and Rayleigh backscattering induced phase noise in the order of $10^{-8}\ rad/\sqrt{Hz}$ [18]) and then amplified by a pre-amplifier (EDFA) (with low noise figure). The passing band of Filter 1&2 (bandwidth of 1nm) matches to that of the probe beam and away from the pump wavelength that is around the P (9) line of acetylene at 1530.37 nm. The minimum detectable phase (MDP) of our system scales inversely with the input optical power in BD (within the detection limit of BD).Thus the use of pre-amplifier EDFA ensures sufficient probe light power reaching the BD, considering the large splicing loss between the SMF and HC-PBF (~4.5 dB per joint here) while remains at low noise level. The use of a FP filter makes the amplified optical power concentrated mainly on the wavelength of interest (1553.33 nm) and avoids the use of a high power laser source which has a much larger coherent length [18].

To minimize the effect of large Fresnel reflection occurring at SMF and HC-PBF joints, an 8° angle is introduced at the end of SMF before it is mechanically spliced to the HC-PBF, as show in Fig. 4(a). The fibre are inserted into a ferrule and then aligned inside a ceramic sleeve with a side slit. A gap of $\sim 5\ \mu m$ is introduced between the SMF and HC-PBF, which allows gas-diffusion into the hollow-core. The transmission loss of this gas cell is ~9 dB while back-reflection is reduced from a few percent down to -35 dB. The two mechanical joints are then sealed in a steel-made T-shaped tube with one end prepared to pressured gas into the HC-PBF.

The MDP of the Sagnac system is firstly examined by the use of a calibrated phase modulator made by wounding ~10.75-m-long SMF around a piezoe-electric transducer (PZT). The PZT phase modulator is placed near the HC-PBF gas cell to generate 5 mrad phase modulation and the corresponding output from ESA is shown in Fig.4 (b), indicating a MDP of $4\times10^{-7}\ rad/\sqrt{Hz}$ at 50 kHz (which is fundamental thermal noise dominant [19]).

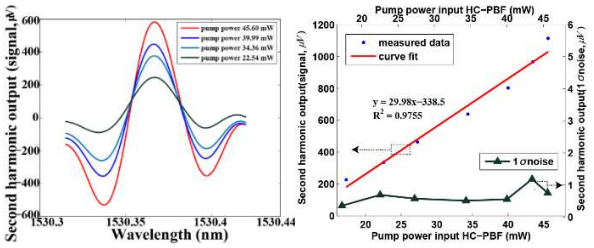

Figure 5, (a) second harmonic lock-in amplifier output waveform when pump wavelength is tuned across the P(9) line 1530.37 nm with different pump power. The C_2H_2 gas concentration is ~100 ppm, pressured into ~1.1-m-long HC-PBF (HC-1550-02, NKT Photonics). (b) second harmonic output signal amplitude and 1σ noise as functions of peak pump power level. The noise was measured with the wavelength of pump beam fixed and tuned away from the absorption line with recording continuously over ~2 min.

Gas detection experiments was then conducted with a 1.1-m-long HC-PBF gas cell filled with 100 ppm C_2H_2. The gas filling was done by applying ~3 atm pressure difference between gas inlet and outlet for ~10 min to ensure the complete filling (even though the theoretical time required is only ~30s [10]). During the experiments, the pressure inside gas cell is at the room temperature and ambient pressure condition.

Fig. 5 (a) shows the second harmonic lock-in output when the pump DFB laser is scanned across the P(9) line of C_2H_2 at 1530.37 nm. The wavelength of DFB is tuned with a slow sawtooth signal (0.005 Hz) through temperature control while its intensity is simultaneously modulated with a fast sinusoidal wave (~24.4 kHz) through current control, which ensures that the second harmonic frequency matches to the proper frequency of the Sagnac loop and at the same time within the optimal frequency of PT phase modulation (i.e. < 330 kHz as discussed above). The amplitude of DFB wavelength modulation is chosen to be as ~2.2 times the linewidth of P(9) line to achieve the best signal-to-noise ratio (SNR). The time constant of lock-in amplifier is set to 1s with 18 dB/oct slope, corresponding to noise equivalent bandwidth 0.094 Hz.

For peak pump power of 45.6 mW, the signal amplitude is ~ $1113.8\,\mu V$ with noise of ~ $0.74\,\mu V$ (1σ level). Thus the noise-equivalent minimum detectable gas concentration is ~ 67 ppb (SNR =1), however which is still worse than the expected calculated value of ~1.4 ppb and may result from the residual amplitude modulation of pump beam [20]. On the other hand, the noise level appears no significant change with pump turned on (~ $0.74\,\mu V$) or off (~ $0.43\,\mu V$), indicating that the pump beam does not introduce extra noise in our system. The lower detection limits with modulation frequency of ~74.2 kHz, 124.5 kHz and 175.2 kHz (all in the optimum frequency of Sagnac loop) were about ~69 ppb, ~148 ppb and ~76 ppb. For higher modulation frequency, the sensitivity would deteriorate which may due to the lower efficient PT effect and also the increase noise of DFB current modulation.

The second harmonic output of signal and 1σ noise level as functions of the peak pump power are shown in Fig. 5 (b). The second harmonic amplitude of lock-in amplifier follows approximately a linear relationship with the peak pump power, while the 1σ noise level presents no significant increase. This implies that further increase of pump power could still improve the detection limit of the gas sensor.

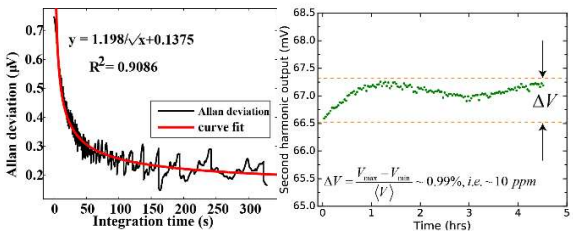

Figure 6 (a) (a) Allan deviation measurement results. The red solid line is the curve fit result with equation $y = A/\sqrt{t} + B$. (b) results of stability test over several hours. The gas concentration is 1000 ppm and all other conditions are identical to what described above. The wavelength of the pump beam is scanned across the absorption line periodically and the maximum value of R-output of lock-in amplifier within every wavelength modulation period is recorded and plotted. The measured was conducted under the normal laboratory condition and environment.

We also conducted the Allan deviation analysis based on the measured second harmonic lock-in output one-hour period when the wavelength of pump is fixed and tuned away from the absorption line. As shown in Fig. 6(a), the Allan deviation decreases with the integration time in the form of $y \propto 1/\sqrt{t}$. We may conclude that the white noise is dominant within the integration time of our measurement [21]. For integration time of 145 s, the Allan deviation is ~ $0.2\,\mu V$, corresponding to the sensitivity of ~18 ppb. These results are much better than previously reported results of direct absorption spectroscopy fibre gas sensor [9, 11] and is comparable to the HC-PBF PTI with a MZI configuration.

The stability of the gas sensor was tested with 1000 ppm gas concentration and the results are shown in Fig. 6(b). The second harmonic output of lock-in amplifier varies <1% over a 4.5-hours-period under laboratory environment, giving a concentration variation of ~10 ppm.

In conclusion, we reported an optimized performance of the photothermal gas spectroscopy by the use of HC-PBF. The frequency-dependent PT effect has been exploited theoretically and experimentally. It has been found that the PT effect remains no significant change with modulation frequency of pump beam smaller than 330 kHz. Based on the choice of optimized modulation frequency, we adapted a modified Sagnac interferometry to achieve a practical gas sensors with sensitivity of C_2H_2 down to 67 ppb (1.1-m-long HC-PBF, 45.6 mW peak pump power) for 1s integration time while could be ~18 ppb for 145 s integration time. The optimized system is comparable with the MZI configuration in terms of sensitivity while possible for a plug-in-play device design. Furthermore, it could be possible for application of multiplex-points sensor network application.

Funding. National Science Foundation (NSF) (1263236, 0968895, 1102301); The 863 Program (2013AA014402)

References

1. B. Culshaw, G. Stewart, F. Dong, C. Tandy, and D. Moodie, Sens. Actuators B **51**, 25-37 (1998).
2. J. M. Fini, Meas. Sci. Technol **15**, 1120-1128 (2004).
3. P. Russell, Science **299**, 358-362 (2003).
4. Y. L. Hoo, W. Jin, C. Shi, H. L. Ho, D. N. Wang, and S. C. Ruan, Appl. Opt **42**, 3509-3515 (2003).
5. A. Cubillas, M. Silva-Lopez, J. Lazaro, O. Conde, M. N. Petrovich, and J. M. Lopez-Higuera, Opt. Express **15**, 17570-17576 (2007).
6. J. C. Knight, Science **282**, 1476-1478 (1998).
7. P. S. J. Russell, P. Hölzer, W. Chang, A. Abdolvand, and J. C. Travers, Nat. Photon **8**, 278-286 (2014).
8. W. Jin, H. F. Xuan, and H. L. Ho, Meas. Sci. Technol **21**, 094014 (2010).
9. F. Yang, W. Jin, Y. Cao, H. L. Ho, and Y. Wang, Opt. Express **22**, 24894-24907 (2014).
10. R. M. Wynne, B. Barabadi, K. J. Creedon, and A. Ortega, J. Lightwave Technol **27**, 1590-1596 (2009).
11. A. M. Cubillas, S. Unterkofler, T. G. Euser, B. J. Etzold, A. C. Jones, P. J. Sadler, P. Wasserscheid, and P. S. Russell, Chem Soc Rev **42**, 8629-8648 (2013).
12. W. Jin, Y. Cao, F. Yang, and H. L. Ho, Nat. Commun **6** (2015).
13. C. C. Davis, and S. J. Petuchowski, Appl. Opt **20**, 2539-2554 (1981).
14. F. Yang, Y. Tan, W. Jin, Y. Lin, Y. Qi, and H. L. Ho, Opt, Lett **41**, 3025-3028 (2016).
15. Y. Lin, W. Jin, F. Yang, J. Ma, C. Wang, H. L. Ho, and Y. Liu, Sci. Rep **6** (2016).
16. Y. L. Hoo, S. Liu, H. L. Ho, and W. Jin, IEEE Photon. Technol **22**, 296-298 (2010).
17. K. Kråkenes, and K. Bløtekjaer, Opt, Lett **14**, 1152-1154 (1989).
18. B. Moslehi, J. Lightwave Technol **4**, 1334-1351 (1986).
19. B. J. Vakoc, M. J. F. Digonnet, and G. S. Kino, Opt. Fiber. Technol **6**, 388-399 (2000).
20. J. Ye, L.-S. Ma, and J. L. Hall, JOSA B **15**, 6-15 (1998).
21. P. Werle, R. Mücke, and F. Slemr, Appl. Phys. B **57**, 131-139 (1993).

1.B. Culshaw, G. Stewart, F. Dong, C. Tandy, and D. Moodie, ''Fibre optic techniques for remote spectroscopic methane detection—from concept to system realisation,'' Sens. Actuators B 51, 25-37 (1998).
2.J. M. Fini, ''Microstructure fibres for optical sensing in gases and liquids,'' Meas. Sci. Technol 15, 1120-1128 (2004).
3.P. Russell, ''Photonic crystal fibers,'' Science 299, 358-362 (2003).
4.Y. L. Hoo, W. Jin, C. Shi, H. L. Ho, D. N. Wang, and S. C. Ruan, ''Design and modeling of a photonic crystal fiber gas sensor,'' Appl. Opt 42, 3509-3515 (2003).
5.A. Cubillas, M. Silva-Lopez, J. Lazaro, O. Conde, M. N. Petrovich, and J. M. Lopez-Higuera, ''Methane detection at 1670-nm band using a hollow-core photonic bandgap fiber and a multiline algorithm,'' Opt. Express 15, 17570-17576 (2007).
6.J. C. Knight, ''Photonic Band Gap Guidance in Optical Fibers,'' Science 282, 1476-1478 (1998).
7.P. S. J. Russell, P. Hölzer, W. Chang, A. Abdolvand, and J. C. Travers, ''Hollow-core photonic crystal fibres for gas-based nonlinear optics,'' Nat. Photon 8, 278-286 (2014).
8.W. Jin, H. F. Xuan, and H. L. Ho, ''Sensing with hollow-core photonic bandgap fibers,'' Meas. Sci. Technol 21, 094014 (2010).
9.F. Yang, W. Jin, Y. Cao, H. L. Ho, and Y. Wang, ''Towards high sensitivity gas detection with hollow-core photonic bandgap fibers,'' Opt. Express 22, 24894-24907 (2014).
10.R. M. Wynne, B. Barabadi, K. J. Creedon, and A. Ortega, ''Sub-minute response time of a hollow-core photonic bandgap fiber gas sensor,'' J. Lightwave Technol 27, 1590-1596 (2009).
11.A. M. Cubillas, S. Unterkofler, T. G. Euser, B. J. Etzold, A. C. Jones, P. J. Sadler, P. Wasserscheid, and P. S. Russell, ''Photonic crystal fibres for chemical sensing and photochemistry,'' Chem Soc Rev 42, 8629-8648 (2013).
12.W. Jin, Y. Cao, F. Yang, and H. L. Ho, ''Ultra-sensitive all-fibre photothermal spectroscopy with large dynamic range,'' Nat. Commun 6 (2015).
13.C. C. Davis, and S. J. Petuchowski, ''Phase fluctuation optical heterodyne spectroscopy of gases,'' Appl. Opt 20, 2539-2554 (1981).
14.F. Yang, Y. Tan, W. Jin, Y. Lin, Y. Qi, and H. L. Ho, ''Hollow-core fiber Fabry–Perot photothermal gas sensor,'' Opt, Lett 41, 3025-3028 (2016).
15.Y. Lin, W. Jin, F. Yang, J. Ma, C. Wang, H. L. Ho, and Y. Liu, ''Pulsed photothermal interferometry for spectroscopic gas detection with hollow-core optical fibre,'' Sci. Rep 6 (2016).
16.Y. L. Hoo, S. Liu, H. L. Ho, and W. Jin, ''Fast response microstructured optical fiber methane sensor with multiple side-openings,'' IEEE Photon. Technol 22, 296-298 (2010).
17.K. Kråkenes, and K. Bløtekjaer, ''Sagnac interferometer for underwater sound detection: noise properties,'' Opt, Lett 14, 1152-1154 (1989).
18. B. Moslehi, "Analysis of optical phase noise in fiber-optic systems employing a laser source with arbitrary coherence time," J. Lightwave Technol 4, 1334-1351 (1986).
19.B. J. Vakoc, M. J. F. Digonnet, and G. S. Kino, ''A Folded Configuration of a Fiber Sagnac-Based Sensor Array,'' Opt. Fiber. Technol 6, 388-399 (2000).
20.P. Werle, R. Mücke, and F. Slemr, ''The limits of signal averaging in atmospheric trace-gas monitoring by tunable diode-laser absorption spectroscopy (TDLAS),'' Appl. Phys. B 57, 131-139 (1993).